Modeling correlated motion in filled skutterudites

Trevor Keiber and Frank Bridges

Modeling Correlated Motion in Filled Skutterudites

Trevor Keiber[1] and Frank Bridges[1]

[1] *Physics Department, University of California, Santa Cruz, California 95064, USA*

Recent extended X-ray absorption fine structure (EXAFS) studies suggest that in skutterudites, the nearly square rings (such as As_4 in $CeFe_4As_{12}$) are quite rigid and may vibrate with low energy modes in one direction, similar to "rattler" atom vibrations. That work suggests that the motions of the square rings and the rattler atoms are coupled. In addition, for $LnCu_3Ru_4O_{12}$, the second neighbor pairs about Ln have stiffer effective springs than the nearest neighbor pairs. To investigate these systems, a one dimensional, four mass, linear chain spring model is developed to describe the recent experimental results, and provide insight about the low energy vibrations in such systems. Our model solves the resulting coupled network of overlapping weak and strong springs and determines the eigenfrequencies and eigenvectors. The dispersion curves show an acoustic mode, two different low energy optical rattling modes involving both the rattler and square, and a non interacting optical mode. Each rattler mode can couple to the acoustic mode, which generates avoided crossings characterized by flattening of the modes; this has important consequences for thermal transport. From these results we calculate atomic correlation functions and the Debye-Waller-like function used in EXAFS, σ^2, as a function of temperature. These calculations show that for the rattler-neighbor pairs, σ^2 is a sum over several modes; it is not the result of a single mode. The inverse slope of $\sigma^2(T)$ at high T provides a measure of the effective spring constants, and the results show that for small direct spring constants the effective spring constant can be significantly larger than the direct spring constants. The locations of the avoided crossings (between rattler modes and the acoustic mode) in q-space can be tuned by the choice of both the rattler and the square atoms. Consequently, it may be possible to further reduce the thermal conductivity using a mixture of nanoparticles, each with avoided crossings at different positions in q-space.

I. INTRODUCTION

The family of skutterudite compounds is growing larger; the frequently studied, filled variety, has the chemical formula LnM_4X_{12} (Ln = lanthanide; M = Fe, Ru, or Os; and X = P, As, or Sb). These compounds display a wide variety of interesting phenomena including low thermal conductivity and good thermoelectric properties at high temperatures, characterized by a high figure of merit, $ZT = TS^2 \frac{\sigma_e}{\kappa_{tot}}$ where S is the Seebeck coefficient, σ_e is the electrical conductivity and κ_{tot} is the thermal conductivity, dominated by the lattice contribution[1–8]. The low thermal conductivity, and hence higher Z in these materials, is generally attributed to the low energy "rattling" motion of the Ln atoms. The unfilled skutterudites such as $CoSb_3$ (Co_4Sb_{12}) have no rattler atoms and have a higher thermal conductivity than the filled compounds[9]. Here we consider primarily filled compounds with a large fraction of the rattler sites occupied.

Skutterudites crystallize in the cubic $Im\bar{3}$ space group, and are characterized by a large unit cell which includes three X_4 squares for every rare earth Ln atom. The transition metal, (M) atoms, and pnictogen (X) atoms form a "cage" surrounding the Ln atom. Oxyskutterudites, such as $LnCu_3Ru_4O_{12}$, are more recently developed materials[10,11], similar to the filled skutterudites, except that the X_4 square is replaced with a CuO_4 group as shown in Fig. 1. The CuO_4 unit is relatively larger, considerably lighter than the X_4 (X = As and Sb) squares, and slightly more rectangular, although we'll continue to refer to CuO_4 as a square.

Recent extended x-ray absorption fine structure (EX-AFS) studies of $CeMAs_{12}$ and $LnCu_3Ru_4O_{12}$ propose that the As_4 and CuO_4 squares are nearly rigid units and that their suspension within the skutterudite structure is anisotropic[12]. The squares are suspended in the unit cell via strong Ru-O or M-As bonds which are quite stiff, but are nearly perpendicular to the square; thus there are strong restoring forces only for motion perpendicular to the squares. There are also moderately large effective spring constants between squares but the resulting restoring forces are mostly perpendicular to the rattler-square axis. Thus the rattler-square system forms weakly connected chain linkages along the x, y, or z directions within a stiffer framework formed of M atoms;[12] vibrations within this linkage should not be considered local modes.

Further support for anisotropic motions of the square rings comes from two other recent EXAFS experiments. In the compound $CePt_4Ge_{12-x}Sb_x$[13] the disorder about Ce, Pt, and Ge for x = 0 is low at 10 K, similar to other skutterudites. However as Sb is added, the environment about Ce becomes disordered, and for x = 3 the peaks are approaching noise levels at 10 K. Thus the Ce-Sb pairs become disordered rapidly. In contrast, for the Pt data, the first Pt-Ge peak remains well ordered and only decreases slightly (25 % at 10K) for x = 3; this bond is nearly perpendicular to the square rings and thus the Ge rings are not displaced significantly in a perpendicular direction. However, the next neighbor Pt-Ge pair, which has a large component in the plane of the squares becomes disordered rapidly with increasing x and at x = 3, the peak is decreases by a factor of 2. This implies motions of the Ge_4 rings within the plane of the rings.
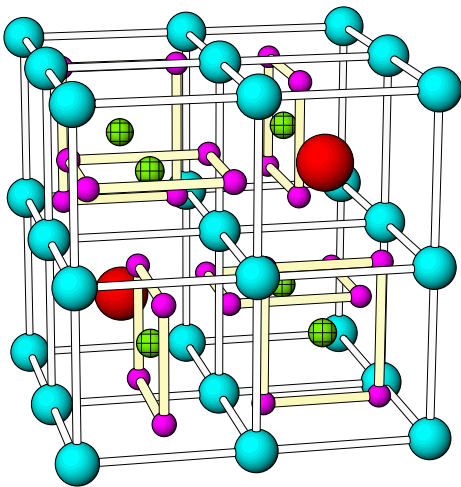
FIG. 1. The structure of an oxyskutterudite, $LnCu_3Ru_4O_{12}$. The light-blue atoms form the cage and usually consist of transition elements such as Fe, Ru, Os. The large red atom is the rare earth rattler atom. The four small purple atoms are oxygen's surrounding the green, (cross-hatched) copper atoms. This square can also consist of four atoms (cross-hatched atom removed) such as As_4, Sb_4 etc. for the filled skutterudites.

For doping on the M site, e.g. $NdFe_{4-x}Ni_xSb_{12}$ or $CeFe_{4-x}Co_xSb_{12}$, the disorder around the Fe site at 10K, remains small with increasing x; instead the largest disorder is again for the neighbors about the rattler atom - the Nd-Sb or Ce-Sb pairs[14]. Thus for both types of substitution - on the squares or on the M sites - the induced local disorder is mostly along the rattler-square axis.

Some of the exotic phenomena observed for these materials originate from the unusual atomic configuration in the large unit cell[15]. Many measurements demonstrate the presence of a low lying optical phonon, supporting the point of view that the Ln ions undergo a low energy "rattling" behavior.[9,16] This low frequency rattling leads to strong effective phonon scattering and is responsible for the extremely low, nearly glass-like, thermal conductivity of these materials[8,17–21]. Keppens et al.[9] noted that there is a higher energy mode that involves Sb atoms in $CeFe_4Sb_{12}$, and theoretical calculations by Feldman et al.[22] find low dispersion optic modes also associated with Sb at somewhat higher energies than the modes associated with the rattler atoms. However the nature of these vibration modes has not been explored.

The early models of the rattler atom motion assumed that large amplitude rattler vibrations inside the cage of rigid atoms would scatters acoustic phonons, thereby reducing the thermal conductivity. Such a vibration would be isotropic in all directions in a weak harmonic potential due to the large amount of space in the cage and cubic symmetry. The rattler equation of motion[12] is then $m_r \frac{d^2u}{dt^2} = -K_{eff}u$ where $K_{eff} = 4\,K_{rs} + 8/3\,K_{rc}$; here K_{rs} is the nearest neighbor and K_{rc} the second neighbor, direct

spring constant. m_r is the rattler mass, within the rigid cage approximation. Others, however, have proposed[23] that m_r should be the reduced mass of the Ln-X pair. Other groups have argued that point defect scattering of acoustic phonons by the rattler atoms is likely not appropriate and one needs to consider how the the rattler motion is coupled to the rest of the lattice[21,22,24].

In a recent study of several Os antimonides[25] ($NdOs_4Sb_{12}$, $PrOs_4Sb_{12}$, and $EuOs_4Sb_{12}$) the vibration amplitude of the rattler, relative to the first and second neighbors (i.e., Nd-Sb and Nd-Os pairs for $NdOs_4Sb_{12}$) did not increase at the same rate with temperature, which is inconsistent with the rigid cage model. The faster increase in vibration amplitude observed for the second neighbor, Nd-Os pair, may not be surprising if one assumes some motion of the Os atoms in the cage; however the Os-Os pair is quite stiff, so how that occurs is not obvious. Further, there is an unusually large static distortion for the Nd-Os pair that is not well understood, but may be related to a cage distortion.[25] Similarly in a series of As skutterudites (CeM_4As_{12}) the Ce-M bond was weaker than the Ce-As bond.[12]

More surprising are the recent results for three oxyskutterudites, ($LnCu_3Ru_4O_{12}$; Ln = La, Pr, and Nd); in these systems the second neighbor Ln-Ru bond is stiffer than the nearest neighbor Ln-O bond.[12] Thus the rigid cage approximation is inadequate for describing the rattler motions in the skutterudites because it predicts the same stiffness for the first and second neighbor bonds, and cannot account for the differences in the rattler behavior for the second neighbor pair, between arsenides and oxyskutterudites.

To gain insight about the local vibrations in rattler systems, Christensen et al.[26] considered the Ba rattler atom in the clathrate, $Ba_8Ga_{16}Ge_{30}$. They introduced a two mass, one dimensional model to described the interaction (coupling) between the rattler optical mode and the acoustic phonon modes. In their paper, the phonon dispersion modes were calculated and compared with experimental results from neutron triple-axis spectroscopy. Their simple model predicted an avoided crossing of the rattler mode and the acoustic-phonon branch. The resulting flattened dispersion curves lead to a significant decrease in the thermal conductivity.

While this model might be sufficient for clathrates, it is insufficient for the skutterudite systems which have both Ln atoms and squares of atoms inside the cage structure. Because of the asymmetric restoring forces on each square, it can move easily towards/away from the rattler, and forms a "second rattler" in the system, which is coupled to the Ln rattler.[12] Thus a model which takes into account the correlated motion of both the Ln rattlers and squares is required.

There are no other simple models involving rattler atom vibrations coupled to the ring atom motions that we are aware of. Several full phonon calculations have been carried out for skutterudites[22,27–31] which show low energy modes with low dispersion, Einstein-like modes;

such modes have been observed directly using inelastic x-ray scattering (IXS) and/or nuclear resonant inelastic scattering (NRIS)[29]. However none of these theoretical studies calculate the Debye-Waller-like parameters, σ^2, used in EXAFS. Considering such low dispersion phonon modes does however raise an important issue - how do the results from direct probes (IXS, NRIS) of these phonon modes compare with atom specific probes that look at the vibrations of a given atom (i.e. atomic displacement parameters (ADP) in diffraction) or the vibrations of atom pairs (σ^2 in EXAFS). The vibration modes probed using IXS and NRIS involve the vibrations of many atoms, while the probes that look at the vibrations of specific atoms or pairs of atoms involves a sum over several modes. We show the latter explicitly in our calculations of σ^2; thus characteristic energies from direct probes of phonon modes (not atom specific) may differ from atom-specific probes.

Here we report a 4-atom unit cell, linear chain model to describe the skutterudite systems in which both the rattler atom and the square rings have weak restoring forces. We consider this the simplest possible model which captures the essential physics of the rattler atom interacting with the square rings and also the cage of surrounding atoms. For this model we calculate the phonon dispersion curves; plots of these dispersion curves illustrate where avoided crossings occur and how they move with changes in parameters. We also calculate $\sigma^2(T)$ for each pair, including the contributions for each mode, and compare the results with recent EXAFS results[12]. The effective spring constant for each pair (Sec. II) is extracted from the inverse slope of $\sigma^2(T)$ at high T.

II. EXPERIMENTAL SPRING CONSTANTS

In recent EXAFS studies of skutterudites[12,23,32–34] the rattler vibrations have been characterized in terms of an Einstein temperature and a static off-set. In the Einstein model the vibrations of the rattler atom are described by one frequency. Although the vibration amplitude (σ^2) is a weighted average over all modes and all of q-space, many details are averaged out. The general equation for $\sigma^2(T)$ in this model is:

$$\sigma^2(T) = \sigma^2_{\text{static}} + \frac{\hbar^2}{2\mu k_\text{B}\theta_\text{E}} \coth \frac{\theta_\text{E}}{2T}, \qquad (1)$$

where θ_E is the Einstein temperature, μ is the effective reduced mass, and σ^2_{static} is the static offset. Within the rigid cage model the effective reduced mass is equal to the mass of the rattler.

Although temperature dependencies are most often reported in terms of an Einstein (or correlated Debye) temperature, EXAFS actually measures an effective spring constant, when in the high T limit.[35] The effective spring constant is a combination of the direct spring constant
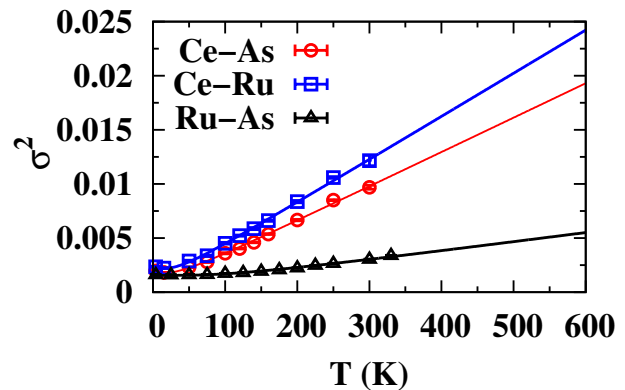

FIG. 2. The experimental values of σ^2 for three atom pairs in $CeRu_4As_{12}$ from Ref. 12 and fits to an Einstein model. These fits were extrapolated to 1000K to obtain K_{rs-eff} and K_{rc-eff}, as well as the much stiffer K_{cc-eff}.

plus a network effect from surrounded bonds. It is denoted by K_{xy-eff}, and should not be confused with the direct spring constant K_{xy} between atoms x and y, which is not directly measurable with EXAFS but is needed for input into the model. To determine the effective spring constants, K_{eff}, from experimental EXAFS data, we use the high temperature approximation to Eqn. 1, given by Eqn. 2. Specifically the Einstein fit of the σ^2 data is extrapolated to high temperatures, and the inverse slope of the data is determined. A similar extrapolation can be used if the data are modeled using a correlated Debye model.[12]

$$K_{eff} = k_B \frac{\Delta T}{\Delta(\sigma^2)} \qquad (2)$$

As an example, experimental $\sigma^2(T)$ results for the Ce-As, Ce-Ru, and As-As pairs[12] in the As skutterudite $CeRu_4As_{12}$ are presented in Fig. 2, and the fits are extrapolated to 1000 K to estimate the effective spring constants using Eqn. 2. K_{rs-eff} and K_{rc-eff} are computed as well as the much stiffer K_{cc-eff}, where rs corresponds to rattler-square, rc to rattler-cage, and cc to cage-cage.

Table I shows the experimentally calculated effective spring constants[12] for filled skutterudites $CeRu_4As_{12}$ and $NdCu_3Ru_4O_{12}$ using the inverse slope of the $\sigma^2(T)$ plot. The cage atom nearest neighbor springs are approximately 2-3 times stiffer than the rattler springs. All comparable bonds of the oxyskutterudites are stronger than the filled skutterudites. This is consistent with the smaller lattice constant of the oxyskutterudites and more tightly bound oxygen bonds. However, the second neighbor Ln-Ru bonds are substantially stiffer than the first neighbor Ln-O bonds which is opposite the results for the filled skutterudites. To estimate the effective spring constant providing the restoring forces for motion in a particular direction, we use the quantity $K_{xy}\cos^2(\theta)$ where θ is the angle between the bond direction and the direc-

tion of motion. For additional spring constant values and further discussion see Ref. 12.

TABLE I. Experimentally calculated effective spring constants[12] for the As skutterudite $CeRu_4As_{12}$ and oxyskutterudite $NdCu_3Ru_4O_{12}$ using the inverse slope of the σ^2 plot. The spring constants for the cage atoms are significantly stiffer than for the springs connected to the rattler atoms. Here "rs" would correspond to Ln-X, "rc" to Ln-Ru, and "cc" approximately to Ru-Ru.

Bond	$CeRu_4As_{12}$ $(eV/Å^2)$	$NdCu_3Ru_4O_{12}$ $(eV/Å^2)$
Ln-X	2.70	4.17
Ln-Ru	2.15	6.50
Ru-X	9.85	13.15
Ru-Ru	4.57	7.17

III. SPRING MODEL

We are primarily interested in the low energy (large amplitude) vibrations along the (100) directions, i.e. between a rattler atom and a square. The relevant part of the unit cell is shown in Fig. 3; it contains one rattler and one square inside the cage atoms. We project all masses and springs onto the (100) axis as shown in Fig. 3b. There are four different masses; m_r represents the rattler mass (in amu), which is nearly the same for the Nd filled oxyskutterudite (144.2) and Ce filled skutterudite (140.1). m_s is the square mass, which is 127.6 for CuO_4 and 299.6 for As_4, while m_c represents a generalized cage mass of four Ru atoms (404.3) and is present twice in the unit cell, separating each square and rattler. In this 1-D projection onto a linear chain it should be noted that in the actual 3-D crystal, the square is the nearest neighbor to the rattler.

Four spring constants are defined in Fig. 3, and only these direct spring constants are input parameters to our model. Further neighbor spring coefficients are weaker, difficult to estimate, and ultimately not needed at this level. The advantage of a system with few parameters is a tractable grasp of the results. The shortcoming is that we have only approximate measures for the springs comprising the system, and a 1-D model. The direct springs used in the model are estimated from the sum of first neighbor pair bonds projected along the (100) axis. There is no easy way to extract exact values of these spring constants, so instead we introduce four generalized direct springs as follows: The spring K_{rs} connects the rattler and square of atoms, corresponding roughly to the two nearest Ln-X bonds projected onto the x-axis, though there are also contributions from other atoms comprising the square. The strength of K_{rs} is much less than the stiff bonds comprising cage-cage interactions. We use a value of 2.2 $eV/Å^2$ for both the As and oxyskutterudites in all calculations. There are two potentially different cage-cage bonds in each unit cell, (one spanning the rattler, and
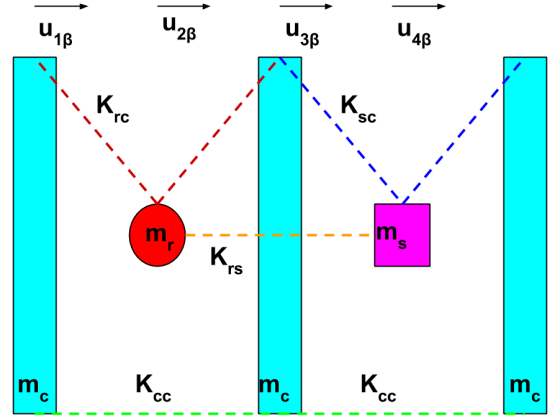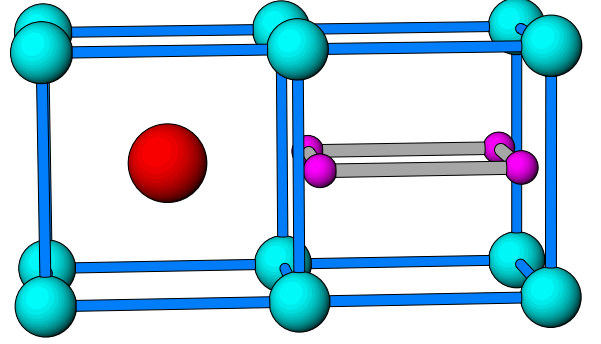

FIG. 3. The top panel shows the rattler and square enclosed by cage atoms forming one quarter of the unit cell along the (100) direction; the lower panel is our symbolic 1-D representation of this part of the unit cell; it is shown expanded vertically for comparison to the top structure but in the model is compressed to a 1-D model. m_r represents the rattler atom mass, (rare earth atom), m_c represents the cage atom mass and is repeated twice per unit cell, and m_s is the mass of the square. K_{cc} is the stiff spring between the cage atoms, K_{rs} is the spring between the rattler and square of atoms (nearest neighbor in 3-D). K_{sc} is the spring which connects the square of atoms to the cage and K_{rc} is the spring constant between the rattler and cage atoms (it corresponds to the rattler second neighbor pair in 3-D). The $u_{i\beta}$ are the displacements of the atoms in the βth unit cell.

the other spanning the square); we set them equal and define them as K_{cc}. This is the strongest bond in the system but difficult to quantify as it represents both Ru-Ru bonds and the projections of two stiff, nearly parallel Ru-X bonds in series. For simplicity we set $K_{cc} = 12$ $eV/Å^2$ for both the As and oxyskutterudites.

Next we define K_{rc} as the spring between the rattler

and cage Ru (or M) atoms. In the 3-D crystal this is related to the second neighbor spring for the rattler; it's relationship to K_{rs} is of primary interest because the strength of this effective bond is one of the major difference between the As and oxyskutterudites. K_{rc} is the projection of four Ln-Ru (Ln-M) bonds onto the x-axis; here we explore several different values for this bond as it effectively couples a one dimensional chain of cage atoms to a one dimensional chain of alternating rattlers and squares. The square to cage bond is K_{sc}, which is similar in nature to K_{rc} as it also couples the motion of the cages to the squares and rattlers. However, the effective spring constant for K_{sc} cannot be directly measured experimentally; it arises from a projection of the restoring forces

from the Ru-As (or Ru-O) spring constants along the 100 direction and is estimated as $K_{Ru-As}\cos^2(\theta)$ where θ is large and $\cos^2(\theta)$ is < 0.1. We expect K_{sc} to be the same order of magnitude as K_{rc}, and we explore a range of values.

The equations of motion for unit cell β with a basis of four atoms are written in terms of the atom coordinates $u_{\alpha\beta}$, where α is the index of the atom within a cell, and β is the index of the unit cell. An example of the equation of motion of the first cage atom motion is shown in Eqn. 3. We change variables to a reduced mass coordinate $z_\alpha(q)$ and utilize the infinite chain model, replacing $u_{\alpha\beta}$ with Eqn. 4, where a is the length of the unit cell.

$$m_c\frac{d^2u_{1\beta}}{dt^2} = -K_{cc}(u_{1\beta} - u_{3\beta}) - K_{cc}(u_{1\beta} - u_{3[\beta-1]}) - K_{rc}(u_{1\beta} - u_{2\beta}) - K_{sc}(u_{1\beta} - u_{4[\beta-1]}) \tag{3}$$

$$u_{\alpha\beta} = \frac{z_\alpha(q)}{\sqrt{m_\alpha}}e^{i(-\omega t + qa\beta + qa(\alpha-1)/4)} \tag{4}$$

From the equations of motion, for a particular wave vector q, we obtain the dynamical matrix in terms of the renormalized coordinates z_α. The matrix that is diagonalized to extract the eigenfrequencies ω_j and eigenstates ϵ_α is given in Eqn. 5.

$$\begin{pmatrix} \frac{2K_{cc}+K_{rc}+K_{rs}}{m_c} & \frac{-K_{rc}e^{iaq/4}}{\sqrt{m_c m_r}} & \frac{-K_{cc}e^{-iaq/2}-K_{cc}e^{iaq/2}}{m_c} & -\frac{K_{sc}e^{-iaq/4}}{\sqrt{m_c m_s}} \\ -\frac{K_{rc}e^{-iaq/4}}{\sqrt{m_c m_r}} & \frac{2K_{rs}+2K_{rc}}{m_r} & -\frac{K_{rc}e^{iaq/4}}{\sqrt{m_c m_r}} & -\frac{K_{rs}e^{-iaq/2}-K_{rs}e^{iaq/2}}{\sqrt{m_r m_s}} \\ \frac{-K_{cc}e^{-iaq/2}-K_{cc}e^{iaq/2}}{m_c} & -\frac{K_{rc}e^{-iaq/4}}{\sqrt{m_c m_r}} & \frac{2K_{cc}+K_{rc}+K_{sc}}{m_c} & -\frac{K_{sc}e^{iaq/4}}{\sqrt{m_c m_s}} \\ -\frac{K_{sc}e^{iaq/4}}{\sqrt{m_c m_s}} & -\frac{K_{rs}e^{iaq/2}-K_{rs}e^{-iaq/2}}{\sqrt{m_r m_s}} & -\frac{K_{sc}e^{-iaq/4}}{\sqrt{m_c m_s}} & \frac{2K_{rs}+K_{sc}}{m_s} \end{pmatrix} \tag{5}$$

IV. AVOIDED CROSSINGS

Before investigating the two-rattler system, it is useful to first consider the eigenfrequency spectrum for the simplified case with no independent motion of the X_4 square. This is done by making K_{rs} and K_{sc} equal to zero, simplifying Eqn. 5 into a 3x3 matrix. In this limit the system is described by three masses per unit cell, m_r and m_c (repeated twice) and two different spring constants K_{cc}, K_{rc}; here K_{rc} plays the role of the weak rattler spring to the rest of the system. This three mass model can be compared to the simple system proposed by Christensen et al.[26] for the clathrates. The dispersion curves for the three mass model are shown in Fig. 4; the lowest mode is the acoustic, the intermediate is the low energy rattler mode and the highest is the non-interacting optical mode. The rattler mode has low energy because of the weak spring (K_{rc}) connecting it to the nearest masses.

Coupling occurs between the acoustic mode and the low energy rattling mode at qa approximately 1.6 radians, which is shown by the avoided crossing in this region, with flattening of the acoustic modes as observed

in the model of Christensen et al.[26]. Flattening of modes has important consequences since the group velocity is the slope of the dispersion curves. Thermal transport is proportional to the group velocity, and if the slope is decreased via mode coupling, then the thermal conductivity will be decreased. The higher optical mode does not couple to the other modes in this calculation and is non-interacting. The location of the avoided crossing is affected by the ratio of the rattler to cage mass, a larger rattler mass shifts the coupling to be closer to the origin. This means that a heavier rattler will effectively scatter phonons at a lower frequency. Additionally, as the ratio of springs K_{rc} to K_{cc} is decreased, the coupling is also shifted nearer to the origin.

In the four mass model, the square - now treated as a large atom - can act as an additional rattler moving in the (100) direction where the restoring forces are smaller; this is especially true for the oxyskutterudites because the CuO_4 square is of comparable mass to the rare earth rattler. There are two potential rattler modes corresponding to different combinations of the vibrations of the lanthanide and square. Each of these can cou-
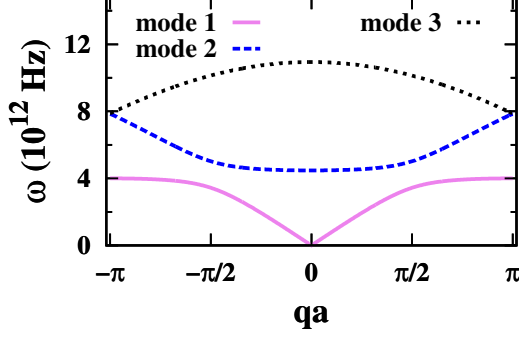
FIG. 4. A plot of the dispersion curves for the system when K_{cc} is significantly larger than K_{rc} for the 3-atom unit cell. The lowest mode is the acoustic, the intermediate is the low energy rattler mode and the highest is the non-interacting optical mode. The interaction between the modes is illustrated by the repulsion (avoided crossing) of the lowest two modes at $qa = 1.6$.

ple to the acoustic mode, creating a more diverse dispersion relation with potentially two crossings instead of one. The two low energy optical modes can interact with each other, and with the acoustic mode, creating several possible avoided crossings. The highest mode is again a non-interacting optical mode for these choices of parameters.

To understand the effect of the spring constants on the dispersion curves and the locations of the avoided crossings, we systematically vary the spring parameters. For comparison purposes, K_{cc} is kept the same and large (12 eV/Å^2) for all figures because the cage-cage spring is always at least 3-5 times larger than the the weaker rattler spring constants. K_{rs} is also kept at a constant value (2.2 eV/Å^2) for all figures, since we are primarily interested in the ratios of $K_{rc}:K_{rs}$ and $K_{sc}:K_{rs}$. In Fig. 5 a grid of nine sets of dispersion curves (appropriate for CeRu$_4$As$_{12}$) are presented, with K_{rc} (horizontal) and K_{sc} (vertical) varied from 0.3 to 2.1 eV/Å^2. In Fig. 6 we present the corresponding figure for the oxyskutterudite which has all of the same spring parameters but a different square mass.

The changes in the curves along the rows of Fig. 5, with K_{sc} constant, shows that increasing K_{rc} shifts the positions of both avoided crossings to higher q values. Additionally, the separation of the modes at the avoided crossing increases with K_{rc}. Along columns, increasing K_{sc} at constant K_{rc}, has a similar though smaller effect, due to the larger square mass.

The locations of the avoided crossings are different for the As and oxyskutterudites mainly because of the different square mass used. A heavier rattler/square mass will cause the avoided crossings to occur nearer to the origin; compare Figs. 5 and 6.
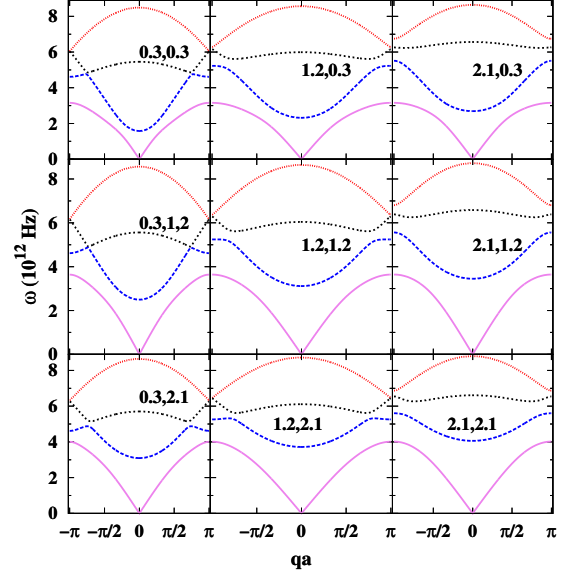

FIG. 5. Plots of different dispersion curves for the As based skutterudite. K_{rc} is varied along the horizontal axis and K_{sc} is varied along the vertical, each from 0.3 to 2.1 eV/Å^2; values of K_{rc}, K_{sc} are given on each panel. There are two avoided crossings in each case, occurring at different wave vector q, depending on the spring constants.

V. CORRELATIONS

It is helpful to consider the correlation functions, $C_{\alpha 1 \alpha 2}(q)$, between atoms at positions α_1 and α_2 in the same unit cell, to understand the relative atomic motions. This function is defined by:

$$C_{\alpha_1 \alpha_2} = \langle u_{\alpha_1} \cdot u_{\alpha_2} \rangle \qquad (6)$$

where $u_{\alpha 1}$ is defined by Eqn. 4. The correlation is positive if the atoms are vibrating in phase, and negative if they are out of phase. For each atom pair (defined by the spring between them) there are four components to the correlation from the four different branches of the dispersion curves as shown in Fig. 7. Because of the avoided crossings, it is difficult to strictly identify some of the various modes (i.e. the acoustic, and the two rattler optic modes) for some values of q. Notice that for each figure the total sum of the positive and negative components cancel for each panel. The dispersion curves are also included at the top, to show how an avoided crossings correspond to features in the correlations. Only the region from $qa=\pm1.8$ is shown to illustrate the first avoided crossing at $qa=0.8$; the second avoided crossing appears as a spike near $qa=2.8$, and is not on this plot.

The cage-cage correlation has a large negative component from mode 4 which is balanced by a positive contribution from modes 1 and 2. Notice that the correlations for mode 1 are larger than for mode 2 near $q = 0$ and transitions to mode 2 when qa is above the position of the
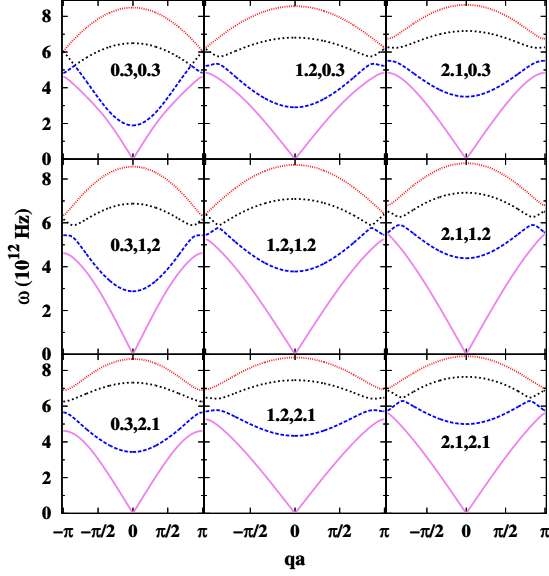
tion from mode 3. The correlation for the rattler-square has a large negative component from mode 3 balanced by positive components from both mode 2 near the origin and mode 1 for $qa > 0.8$. There is almost no contribution from mode 4. The correlations for the rattler-cage is similar to that for the square-cage; for each, the correlation is negative for mode 2 and positive (with the same magnitude) for mode 1.

FIG. 6. The dispersion curves for the oxyskutterudite, with the square mass equal to that of the CuO_4 unit. K_{rc} is again varied along the horizontal axis and K_{sc} along the vertical. The two avoided crossings occur at different wave vectors q than in Fig. 5.

avoided crossing at $qa = 0.8$. There is negligible contribu-

VI. THERMAL BROADENING

The average thermal motion as a function of temperature for a pair of atoms is quantified by $\sigma^2(T)$, defined in Eqn. 7, where σ is the width of the pair distribution function. This is a parameter which EXAFS can measure, and as discussed in section II, we can use the inverse slope of $\sigma^2(T)$ in the high T limit, to calculate effective spring constants.

Using the eigenvalue analysis we can determine the contribution for each mode and q-vector; These contributions are multiplied by the thermal occupation for each state based on the energy, $\hbar\omega_j(q)$, and integrated over all wave vectors q, as shown in Eqn. 8. We sum over the four branches of the dispersion curves to get the total σ^2 for a pair, though it is useful to look at each mode independently.

$$\sigma^2_{\alpha_1\alpha_2} = \left\langle |u_{\alpha_1} - u_{\alpha_2}|^2 \right\rangle. \tag{7}$$

$$\sigma^2_{\alpha1,\alpha2}(T) = \sum_{j=1}^{4} \int \left| \frac{\epsilon_{\alpha1,j}(q)}{\sqrt{m_{\alpha1}}} - \frac{\epsilon_{\alpha2,j}(q)}{\sqrt{m_{\alpha2}}} \right|^2 \frac{\hbar}{2\omega_j} \coth\frac{\omega_j\hbar}{k_B T} dq \tag{8}$$

The values of the components of σ^2 as a function of temperature for each pair are shown in Fig. 8 along with the sum of all of the components. This figure uses the same parameters as the correlation functions. In panel one, the overall amplitude of σ^2_{cc} is quite low relative to the other pairs, which is characteristic of the stiff cage to cage bond. The largest component of σ^2_{cc} is from mode 4 which is the highest optical mode. In panel two, σ^2_{rs} is substantially larger than σ^2_{cc}, but slightly smaller in magnitude than σ^2_{rc} and σ^2_{sc}. The largest component in panel two is from mode 3 followed by mode 1 and mode 2 with almost none from mode 4. σ^2_{rc} in panel 3 and σ^2_{sc} in panel 4 have approximately equal slopes, which is expected since they have the same initial spring constants. Each has the most significant contribution from mode 2 and very little contribution from mode 4. σ^2_{rc} has contributions from both mode 1 and 3 while σ^2_{sc} has a significant contribution from mode 1 but little from mode 3. Note that because of the mixing of modes the

nature of mode 1 changes from an acoustic mode to a rattler mode as qa increases; similar cross-overs occur for modes 2 and 3 at higher qa. These plots show explicitly that the vibration amplitude for atom pairs is a sum over two or more modes and hence a characteristic energy will be some weighted average of several modes. The average energy may not be very close to the dominant optic mode energy.

In Fig. 9a, $\sigma^2(T)$ is plotted for the first four neighbors in $CeRu_4As_{12}$ from simulations using the spring model. The slope for the Ce-Ru pair (K_{rc-eff}) is greater than that for the the Ce-As pair (K_{rs-eff}), implying a weaker second neighbor bond as observed. The slope for the Ru-Ru pair (K_{cc-eff}) is much lower indicating a stiff bond. In part (b) the $\sigma^2(T)$ plots correspond to pairs in $NdCu_3Ru_4O_{12}$. Here the slope for the Nd-Ru pair (K_{rc-eff}) is less than that for the Nd-O pair (K_{r-effs}), which means the first neighbor bond is weaker than the second neighbor bond, in contrast to the re-
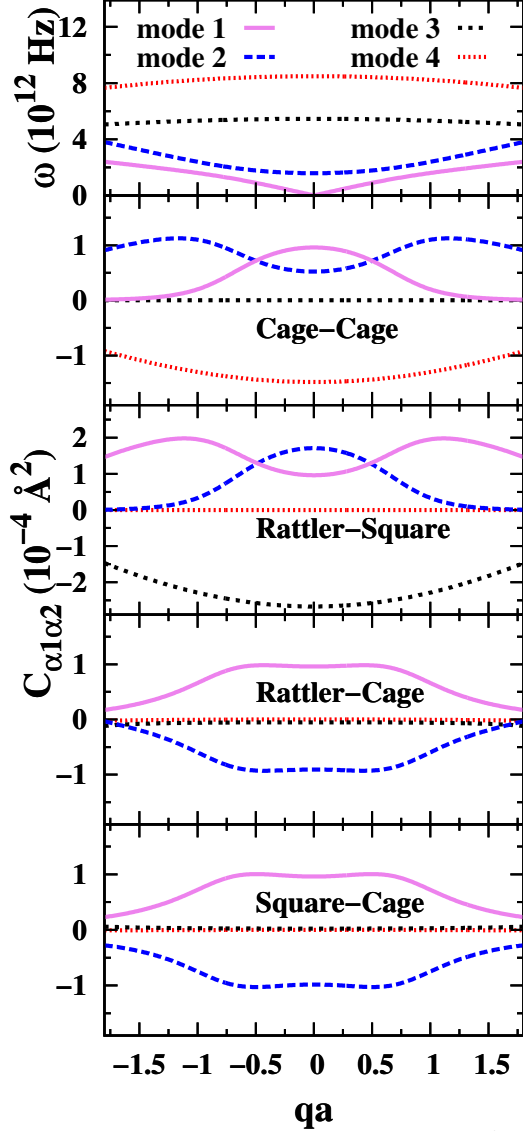
FIG. 7. The dispersion curves corresponding to the As Skutterudite are shown in the top panel for the restricted qa range -1.8 to 1.8 (K_{rc}=0.3, K_{sc}=0.3). This figure highlights the avoided crossing at qa=0.8; a second crossing (between mode 2 and 3) at $qa = 2.8$ is not shown. The second panel shows the components of the correlation function for K_{cc}. The third, fourth, and fifth panels correspond to K_{rs}, K_{rc} and K_{sc}. Positive correlations mean the pair of atoms move in the same direction for a given mode; negative correlations mean they move in opposite directions.

FIG. 8. The components of σ^2 are shown as a function of temperature for each atomic pair, using the calculation appropriate for CeRu$_4$As$_{12}$. In panel one the components of σ^2_{cc} (Ru-Ru) are shown and in panels two, three, and four σ^2_{rs} (Ce-Sb), σ^2_{rc} (Ce-Ru), and σ^2_{sc} are shown; the latter corresponds to the effective restoring force along a 100 direction in the cubic unit cell from the projected component of the Ru-Sb bonds. The sum of all modes in a panel is shown as the dot-dash curve; this should be comparable to the experimental curve.

sult for the As skutterudite, but consistent with experiments on oxy-skutterudites. Note that K_{sc-eff} has approximately the same stiffness as K_{rc-eff} (triangles and squares on Fig. 9); however, both are much larger than the direct bonds K_{sc} or K_{rc} used to calculate the dispersion curves. K_{cc-eff} is much stiffer than the other bonds and is almost unchanged from the value for the direct spring constant K_{cc}. Einstein fits were applied to the rattler pairs and are in good agreement with experi-
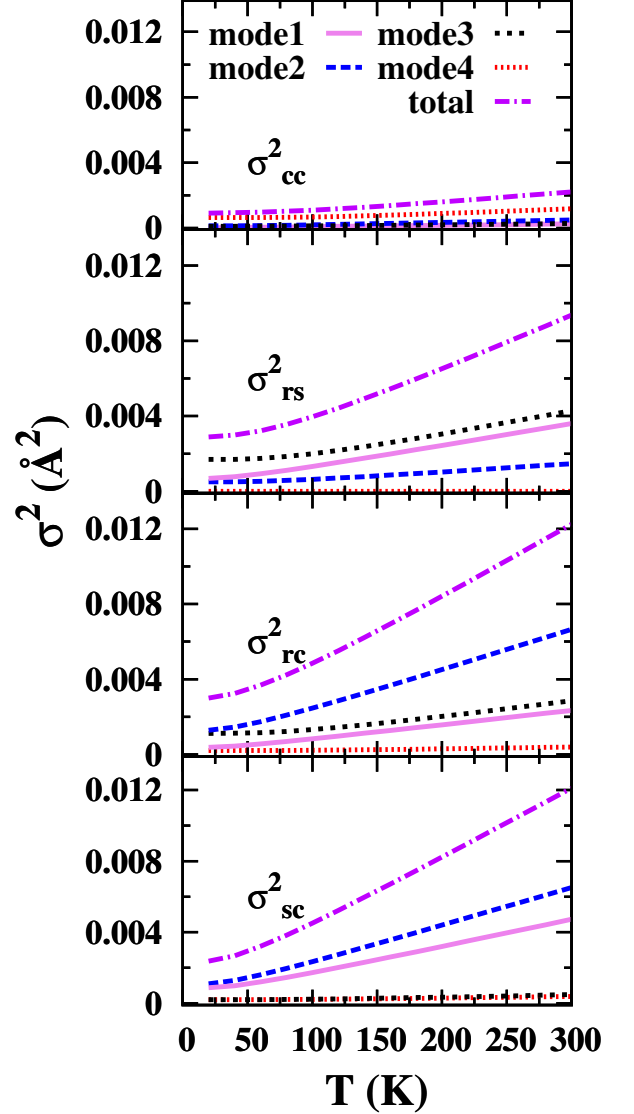
mental results.

VII.   EFFECTIVE SPRING CONSTANTS

The effective spring constants were determined from the inverse slope of the σ^2 data as in Sec. II. Different cage masses do not significantly change the effective spring constants when they are calculated from the high
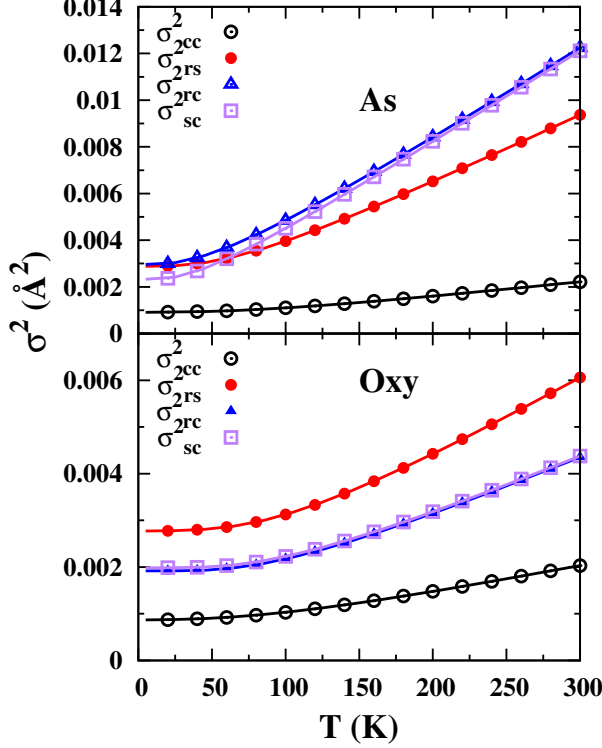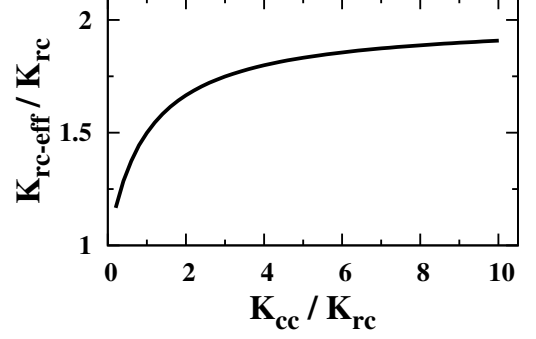
FIG. 10. The variation of K_{rc-eff} as the ratio of K_{cc} to K_{rc} increases. As K_{cc} becomes much larger than K_{rc}, the value of K_{rc-eff} goes to $2K_{rc}$. When K_{cc} becomes much less than K_{rc} the value of $K_{rc-eff} = K_{rc}$.

FIG. 9. (a) $\sigma^2(T)$ functions, calculated from the spring model for the first few neighbor pairs in $CeRu_4As_{12}$; $K_{rc} = K_{sc} = 0.3$ eV/Å^2. The slope for the Ce-Ru pair (K_{rc}) is greater than for the Ce-As pair ((K_{rs})), implying a weaker bond. (b) Calculated $\sigma^2(T)$ functions for pairs in $NdCu_3Ru_4O_{12}$ are shown. The slope for Nd-Ru (K_{rc}) is less than that for Nd-O (K_{rs}) which indicates that the Nd-Ru effective bond is stronger than the effective Nd-O bond. The solid lines are fits to an Einstein model for $\sigma^2_{rs}(T)$, $\sigma^2_{rc}(T)$, and $\sigma^2_{sc}(T)$, and to a correlated Debye model for $\sigma^2_{cc}(T)$.

temperature slopes of $\sigma^2(T)$ (with direct spring constants fixed). This result at first may seem counter-intuitive but is a fundamental feature of the system. Changing the ratio of masses instead changes the zero point motion contributions which are measured by the y-intercepts on the $\sigma^2(T)$ data at T = 0; i.e. σ^2(T=0). Smaller rattler masses have greater zero point motion than larger masses. The ratio of the direct spring constants used as input to the model, determines the effective spring constants in a non-trivial way.

To understand the relationship between the direct spring constants and effective spring constants it is instructive to once again turn to the simplified three mass system (the square mass is remove by setting K_{rs} and K_{sc}=0). As the ratio of the direct spring constants K_{rc} to K_{cc} is varied, the value of K_{rc-eff} changes as shown in Fig. 10. As K_{cc} becomes much larger than K_{rc} then we approximate a rigid cage model and the value of K_{rc-eff} approaches $2*K_{rc}$. For the case where K_{cc} is less than

K_{rc} the value of K_{rc-eff} approaches K_{rc}.

For the four mass system, the relationship between effective and direct spring constants is more complex. To illustrate the behavior we keep K_{rs} at 2.2 eV/Å^2 and K_{cc} at 12 eV/Å^2, determining all effective spring constants as a function of changing K_{rc} and K_{sc}. In table II each of the four effective spring constants is shown as K_{rc} (rows) and K_{sc} (columns) are incremented (0.3 to 1.2 to 2.1). Since the square mass has no significant contribution to the spring constants, this table is the same whether using the As$_4$ or CuO$_4$ square. K_{cc-eff} is not significantly different from K_{cc} ($< 6\%$), and remains much larger than any of the other effective spring constants. K_{rs-eff} is approximately 25% larger than K_{rs} for small values of K_{rc} and K_{sc}, and is nearly a factor of 2 larger for the largest values of K_{rc} and K_{sc} considered. K_{rc-eff} and K_{sc-eff} are each much larger than their direct spring constant values for any values in the table, having significant contributions from the networks of springs.

The ratio of the second neighbor to first neighbor, direct spring constants, (i.e. K_{rc}:K_{rs} and K_{sc}:K_{rs}) determines whether the effective second neighbor spring constant is larger or smaller than the first neighbor. When these ratios are small enough, the first neighbor effective spring constant K_{rs-eff} is largest. Therefore, the upper left corner of Table II, with small values of K_{sc} and K_{rc}, is more like the As skutterudite systems while the lower right of the table, with larger ratios is more like the oxyskutterudites. The most important factor influencing the magnitude of the ratio of the first to second neighbor effective spring constants from the rattler or square is the ratio of the same direct neighbor spring constants. There is a smooth transition from the As-skutterudite-like behavior to oxyskutterudite-like behavior, with intermediate ratios yielding nearly equal first and second neighbor effective spring constants.

Fig. 11 shows the effect of varying K_{rc} on the effective spring constants, K_{rs-eff}, K_{rc-eff} and K_{sc-eff}.

TABLE II. The four effective spring constants, calculated for the As Skutterudite system, are tabulated as a function of both K_{rc} and K_{sc}, simulating a variety of possible results. Using the oxyskutterudite square mass gives nearly identical values. K_{sc} is varied horizontally and K_{rc} is varied vertically. The upper left corner is more like the As skutterudite system while the lower right is more like the oxyskutterudites. All entries are in units of eV/Å^2, $K_{cc} = 12$ eV/Å^2, $K_{rs} = 2.2$ eV/Å^2.

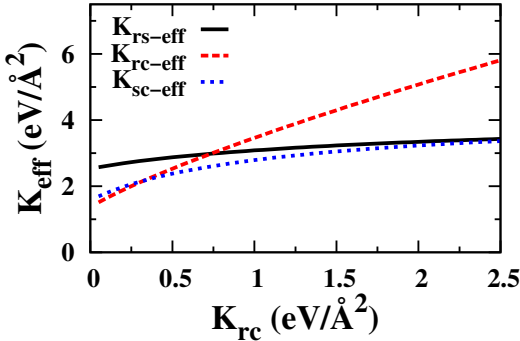|	Bond	$K_{sc} = 0.3$	$K_{sc} = 1.2$	$K_{sc} = 2.1$
$K_{rc-eff} = 0.3$	K_{cc}	11.67	11.85	11.94
	K_{rs-eff}	2.76	3.15	3.36
	K_{rc-eff}	2.11	2.87	3.21
	K_{sc-eff}	2.13	3.87	5.36
$K_{rc-eff}=1.2$	K_{cc}	12.10	12.25	12.34
	K_{rs-eff}	3.15	3.65	3.97
	K_{rc-eff}	3.80	4.36	4.64
	K_{sc-eff}	2.91	4.45	5.85
$K_{rc-eff}=2.1$	K_{cc}	12.51	12.65	12.72
	K_{rs-eff}	3.36	3.97	4.37
	K_{rc-eff}	5.22	5.69	5.94
	K_{sc-eff}	3.26	4.74	6.11

FIG. 11. Changes of effective spring constants as a function of K_{rc} with K_{cc}, K_{rs}, and K_{sc} held fixed at 12, 2.2 and 0.3 eV/Å^2 respectively. Notice that increasing K_{rc} has a larger effect on K_{rc-eff}, and that K_{rs-eff} (first neighbor in 3D) and K_{rc-eff} (second neighbor in 3D) cross near $K_{rc} = 0.75$.

K_{cc-eff} is not shown since it remains much larger than the other effective spring constants and is nearly unchanged. Notice that increasing K_{rc} has the largest effect on K_{rc-eff}; it increases monotonically with K_{rc}. The effect is smaller for K_{rs-eff} and K_{sc-eff}. The figure clearly shows where K_{rs-eff} and K_{rc-eff} cross; for these parameters, it occurs when the direct spring constant $K_{rc} \sim 0.75$ eV/Å^2. If one varies K_{sc} instead of K_{rc}, the plots are nearly identical except that K_{sc-eff} and K_{rc-eff} are switched with K_{sc-eff} having the greater slope.

VIII. DISCUSSION AND CONCLUSIONS

We present a relatively simple 4-atom model that provides a means of exploring the vibrational properties of a system with overlapping weak and strong springs. The system can be viewed as two infinite chains (each with 2-atom unit cells) coupled together via weak springs. The

equations of motion were solved numerically to obtain the dispersion curves and the corresponding eigenvalues. The four resulting modes correspond roughly to an acoustic mode, two low energy optic modes (rattler modes) and a high energy optic mode, which plays little role in the low energy properties. In addition, there is strong coupling between the acoustic and the two low energy optic modes leading to avoided crossings and dispersion curves with low slopes. This results in a low velocity of sound, which is beneficial for thermoelectric applications. The location of the coupling in q-space is affected by the spring constants and masses used; for example, a larger rattler mass shifts the coupling closer to the origin.

Once the eigenfrequencies and eigenvalues are known as a function of the wavevector q, a number of useful quantities can be calculated; these include the correlation functions which show the relative motions of pairs of atoms, σ^2 as a function of temperature which can be compared with experiment, and effective spring constants. The latter can be extracted from plots of σ^2 vs T in the same way as for experimental data. We find that the strongest effective spring constants within the cage are nearly identical to the direct spring constants used as input for the model. However when the direct spring constant is small compared to other spring constants, the effective spring constant for that pair can be much larger. Thus the ratios of effective spring constants depend on the direct spring constants, in a non-trivial way. For the intermediate spring constant K_{rs} the effective spring constant is about 25% larger for parameters corresponding the the As skutterudite and about a factor of two larger for the model for the oxyskutterudites. As the rattler-cage direct spring constant is increased, the second neighbor effective spring constant, K_{rc-eff}, varies from being smaller than the rattler-square effective spring constant, K_{rs-eff}, to being larger than K_{rs-eff}, although for the direct spring constants, K_{rc} is smaller than K_{rs}. Thus the unusual differences for the As skutterudites and the oxyskutterudites can be understood using this model.

An important feature of this model is that the square

ring also acts as a rattler and introduces additional coupling with the acoustic modes, which further reduces the thermal conductivity. Treating the square rings as nearly rigid units is a simplifying approximation, but because the bonds within the square rings are the second strongest in the structure, we consider it is a reasonable approximation for low energy modes. We have observed evidence for low energy motion of the square rings along the rattler-square axis for many systems – arsenides, oxy-skutterudites, antimonides including doped materials, and the $CePt_4Ge_{12}$ system. Thus we propose that this behavior is a general feature of the skutterudite structure. It would be useful in full calculations of the phonon modes to project the motions of the ring atoms along various directions and investigate correlations for the low energy modes. If the rings are quasi-rigid as proposed here, the motions of the four ring atoms will be highly correlated.

An interesting and potentially important result from these studies is that one should have two avoided crossing between acoustic and low energy rattler modes, and that the positions of these avoided crossings in q space can be tuned by changing masses or spring constants. Consequently if the material consists of many nanodomains, with different positions of the avoided crossings, phonon transport may be highly suppressed; acoustic phonons of a given frequency and q-vector that propagate freely in one domain, cannot propagate in another region that has an avoided crossing at that q-vector.

Thus if large nanoparticles (100-300 nm) containing significantly different rattler masses or square ring masses, are optimized to have a large power factor $S^2\sigma_e$, then a mixture of such nanoparticles should lead to a low thermal conductivity; some nanoparticles might also be unfilled[20]. The improved performance of some multiply filled skutterudites[8,36–46] may be explained in part from nanodomains with avoided crossings at different q-vectors. However, in many cases the concentrations of some filler atom are low and in that case defect scattering should also play an important role. To separate mechanisms it would be useful to compare a multiply filled material with a mixture of singly filled nanoparticles with the same average composition.

We anticipate that this simple model will encourage experiments using a mixture of nanoparticles as well as motivate theoretical calculation to look for correlated motions of the ring atoms and investigate transport in inhomogeneous materials containing many nanodomains.

IX. ACKNOWLEDGMENTS

[1] B. C. Sales, D. Mandrus, and R. K. Williams, Science **272**, 1325 (1996).

[2] B. C. Sales, D. Mandrus, B. C. Chakoumakos, V. Keppens, and J. R. Thompson, Phys. Rev. B **56**, 15081 (1997).

[3] G. D. Mahan, Solid State Phys. **51**, 81 (1998).

[4] B. C. Sales, in Handbook on the Physics and Chemistry of Rare Earths, edited by L. Eyring, K. A. Gschneidner, and G. H. Lander (Elsevier Science Publishing Co., New York, 2003), Vol. 33, Chap. 211, pp. 1–34.

[5] G. S. Nolas, J. L. Cohn, G. A. Slack, and S. B. Schujman, Appl. Phys. Lett **73**, 178 (1998).

[6] A. J. Minnich, M. S. Dresselhaus, Z. F. Ren, and G. Chen, Energy Environ. Sci. **2**, 466 (2009).

[7] M. B. Maple, R. E. Baumbach, J. J. Hamlin, P. C. Ho, L. Shu, D. E. MacLaughlin, Z. Henkie, R. Wawryk, T. Cichorek, and A. Pietraszko, in Properties and Applications of Thermoelectric Materials, NATO Sci. Peace Sec. Series B: Physics and Biophysics, edited by V. Zlatic and A. C. Hewson (Springer, Netherlands, 2009), pp. 1–18.

[8] X. Shi, J. Yang, J. R. Salvador, M. Chi, J. Y. Cho, H. Wang, S. Bai, J. Yang, W. Zhang, and L. Chen, J. Am. Chem. Soc **133**, 7837 (2011).

[9] V. Keppens, D. Mandrus, B. C. Sales, B. C. Chakoumakos, P. Dai, R. Coldea, M. B. Maple, D. A. Gajewski, E. J. Freeman, and S. Bennington, Nature **395**, 876 (1998).

[10] S. G. Ebbinghaus, A. Weidenkaff, and R. J. Cava, J. Solid State Chem. **167**, 126 (2002).

[11] A. N. Vasil'ev and O. S. Volkova, Low Temp Phys. **33**, 895 (2007).

[12] F. Bridges, B. Car, L. Sutton, M. Hoffman-Stapleton, T. Keiber, R. E. Baumbach, M. B. Maple, Z. Henkie, and R. Wawryk, Phys. Rev B **91**, 014109 (2015).

[13] F. Bridges, P. Nast, J. Wilde, T. Keiber, M. B. Maple, K. Huang, and B. D. White, IOP Conf. Ser.: Mat. Sci. Engin. **80**, 012004 (2015).

[14] F. Riva, A. Miler, and F. Bridges (unpublished).

[15] G. J. Snyder and E. S. Toberer, Phys. Rev. B **7**, 105 (2008).

[16] C. H. Lee, I. Hase, H. Sugawara, H. Yoshizawa, and H. Sato, J. Phys. Soc. Jpn. **75**, 123602 (2006).

[17] K. Hattori, Y. Hirayama, and K. Miyake, Journal of the Physical Society of Japan **74**, 3306 (2005).

[18] S. Yashiki, S. Kirino, K. Hattori, and K. Ueda, J. Phys. Soc. Jpn. 80 **80**, 130 (2011).

[19] W. Zhao, P. Wei, Q. Zhang, H. Peng, W. Zhu, D. Tang, J. Yu, H. Zhou, Z. Liu, X. Mu, D. He, J. Li, C. Wang, X. Tang, and J. Yang, Nat. Comm. **6**, 6197 (2014).

[20] H. Chi, H. Kim, J. C. Thomas, X. Su, S. Stackhouse, M. Kaviany, A. V. Ven, X. Tang, and C. Uher, Phys. Rev. B **86**, 195209 (2012).

[21] M. M. Koza, M. R. Johnson, R. Viennois, H. Mutka, L. Girard, and D. Ravot, Nature Mater. **7**, 805 (2008).

[22] J. L. Feldman, D. J. Singh, I. I. Mazin, D. Mandrus, and B. C. Sales, Phys. Rev. B **61**, R9209 (2000).

[23] K. Nitta, Y. Omori, D. Kikuchi, T. Miyanaga, K. Takegahara, H. Sugawara, and H. Sato, J. Phys. Soc. Jpn. **77**, 063601 (2008).

[24] W. Li and N. Mingo, Phys. Rev. B **89**, 184304 (2014).

[25] T. Keiber, F. Bridges, R. E. Baumbach, and M. B. Maple, Phys. Rev. B **86**, 174106 (2012).

[26] M. Christensen, A. B. Abrahamsen, N. B. Christensen, F. Juranyl, N. H. Andersen, K. Lefmann, J. Andreasson, and C. R. H. Bahl, Nat. Mat. **7**, 811 (2008), dOI: 10.1038/nmat2273.

[27] J. L. Feldman, D. J. Singh, C. Kendziora, D. Mandrus, and B. C. Sales, Phys. Rev. B **68**, 094301 (2003).

[28] J. L. Feldman, P. Dai, T. Enck, B. C. Sales, D. Mandrus, and D. J. Singh, Phys. Rev. B **73**, 014306 (2006).

[29] S. Tsutsui, H. Kobayashi, D. Ishikawa, J. P. Sutter, A. Q. R. Baron, T. Hasegawa, N. Ogita, M. Udagawa, Y. Yoda, H. Onodera, D. Kikuchi, H. Sugawara, C. Sekine, I. Shirotani, and H. Sato, J. Phys. Soc. Jpn. **77**, 033601 (2008).

[30] N. Bernstein, J. L. Feldman, and D. J. Singh, Phys. Rev. B **81**, 134301 (2010).

[31] J. L. Feldman, D. J. Singh, and N. Bernstein, Phys. Rev. B **89**, 224304 (2014).

[32] D. Cao, F. Bridges, P. Chesler, S. Bushart, E. D. Bauer, and M. B. Maple, Phys. Rev. B **70**, 094109 (2004).

[33] D. Cao, R. H. Heffner, F. Bridges, I.-K. Jeong, E. D. Bauer, W. M. Yuhasz, and M. B. Maple, Phys. Rev. Lett. **94**, 036403/1 (2005).

[34] M. Mizumaki, S. Tsutsui, T. Uruga, H. Tanida, D. Kikuchi, H. Sugawara, and H. Sato, J. Phys. Soc. Jpn. **80**, 074603/1 (2013).

[35] B. K. Teo, <u>EXAFS: Basic Principles and Data Analysis</u> (Springer-Verlag, New York, 1986).

[36] D. Berardan, E. Alleno, C. Godart, M. Puyet, B. Lenoir, R. Lackner, E. Bauer, L. Girard, and D. Ravot, J. Appl. Phys. **989**, 033710 (2005).

[37] E. Alleno, D. Berardan, C. Godart, M. Puyet, B. Lenoir, R. Lackner, E. Bauer, and D. R. L. Girard, Physica B **383**, 103 (2006).

[38] J. Yang, W. Zhang, S. Q. Bai, Z. Mei, and L. D. Chen, App. Phys. Lett. **90**, 192111 (2007).

[39] S. Q. Bai, Y. Z. Pei, L. D. Chen, W. Q. Zhang, X. Y. Zhao, and J. Yang, Acta Mater. **57**, 3135 (2009).

[40] G. Rogl, A. Grytsiv, E. Bauer, P. Rogl, and M. Zehetbauer, Intermet. **18**, 394 (2010).

[41] G. Rogl, L. Zhang, P. Rogl, A. Grytsiv, M. Falmbigl, D. Rajs, M. Kriegisch, H. Mller, E. Bauer, J. Koppensteiner, W. Schranz, M. Zehetbauer, Z. Henkie, and M. B. Maple, J. App. Phys. **107**, 043507 (2010).

[42] J. Peng, W. Xu, Y. Yan, J. Yang, L. Fu, H. Kang, , and J. He, J. Appl. Phys. **112**, 024909 (2012).

[43] Y. G. Yan, W. Wong-Ng, L. Li, I. Levin, J. A. Kaduk, M. R. Suchomel, X. Sun, G. J. Tan, and X. F. Tang, J. Solid state Chem. **218**, 221 (2014).

[44] J. Yu, W.-Y. Zhao, P. Wei, W.-T. Zhu, H.-Y. Zhou, Z.-Y. Liu, D.-G. Tang, B. Lei, and Q.-J. Zhang, Appl. Phys. Lett. **104**, 142104 (2014).

[45] G. Rogl, A. Grytsiv, P. Rogl, N. Peranio, E. Bauer, M. Zehetbauer, and O. Eibl, Acta Mater **63**, 30 (2014).

[46] G. Rogl, A. Grytsiv, P. Rogl, E. Bauer, M. Hochenhofer, R. Anbalagan, R. C. Mallik, and E. Schafler, Acta Mater **76**, 434 (2014), http://dx.doi.org/10.1016/j.actamat.2014.05.051.